Int J Fract (2017) 206:1–10
DOI 10.1007/s10704-017-0193-3

ORIGINAL PAPER

Effect of cooperative grain boundary sliding and migration on dislocation emission from a branched crack tip in deformed nanocrystalline solids

Tengwu He · Wanshen Xiao · Yan Zhang · Haiping Zhu

Received: 9 April 2016 / Accepted: 2 February 2017 / Published online: 14 March 2017

Abstract A theoretical model is established to describe the effect of cooperative grain boundary (GB) sliding and migration on dislocation emission from the tip of branched crack in deformed nanocrystalline solids. The explicit solutions of complex potentials are obtained by means of complex variable method and conformal mapping technique. The critical stress intensity factors (SIFs) for the first lattice dislocation emission from the tip of branched crack are calculated. The effects of the lengths of branched crack and main crack, and the angle between their planes on the critical SIFs for dislocation emission are evaluated in detail. The results indicate that the emission of lattice dislocations from the tip of branched crack is strongly influenced by cooperative GB sliding and migration. When main crack approaches the branched crack, dislocation emission from the tip of branched crack will be suppressed. The main crack tends to propagate while shorter branched crack is prone to be blunted by emitting lattice dislocations from its tip. As a special case, when the planes of main crack and the branched crack are flattened out into one, the present results are in good agreement with previously known results.

Keywords Branched crack · Cooperative grain boundary sliding and migration · Dislocation emission · Nanocrystalline solids · Conformal mapping · Stress intensity factors

T. He · W. Xiao (✉) · Y. Zhang
College of Mechanical and Vehicle Engineering, Hunan University, Changsha 410082, Hunan Province, People's Republic of China
e-mail: xwshndc@126.com

H. Zhu
School of Computing, Engineering and Mathematics, University of Western Sydney, Locked Bag 1797, Penrith, NSW 2751, Australia

1 Introduction

Nanocrystalline materials display unusual mechanical and physical properties that have attracted a wide range of technological applications (Xu et al. 2013; Feng et al. 2013a; Ovid'Ko and Sheinerman 2010; Aifantis 2011; Zhou et al. 2008; Zhu et al. 2012; Wolf et al. 2005; Sergueeva et al. 2009; Mukhopadhyay and Basu 2007; Meyers et al. 2006; Zhu and Zheng 2010; Wu et al. 2007; Farrokh and Khan 2009; Barai and Weng 2009; Bobylev et al. 2009; Xia and Wang 2010). In most cases, they are generally characterized by high strength, strong hardness and excellent wear resistance but low tensile ductility and low fracture toughness at room temperature, which severely narrows their practical applications (Yinmin et al. 2002; Youssef et al. 2005; Dao et al. 2007; Ovid'Ko and Sheinerman 2012). Nevertheless, some recent examples of nanocrystalline materials showing considerable tensile ductility at room temperature or superplasticity at elevated temperature and improvement of fracture toughness have been detected and reported (Ovid'ko

and Sheinerman 2007; Zhao et al. 2004; Bhaduri and Bhaduri 1997; Youssef et al. 2006; Ovid'Ko et al. 2008). They evoke high interest of many scholars and practitioners in exploring the fundamentals of special toughening mechanisms in nanocrystalline materials. Subsequently, many theoretical models such as GB sliding, GB migration, rotational deformation, twinning and triple junction diffusion creep, have been extensively developed to account for the toughening mechanisms of nanocrystalline materials (Bobylev et al. 2010, 2011; Gutkin and Ovid'Ko 2005; Juan et al. 2012; Morozov et al. 2010).

In recent years, rapidly growing attention has been concentrated on cooperative GB sliding and stress-driven migration in nanocrystalline materials, which represents a new toughening mechanism and a special deformation mechanism compared to pure GB sliding (Bobylev et al. 2010). This view is supported by large numbers of experimental observations (Dao et al. 2007; Sergueeva et al. 2006, 2007) and theoretical results (Gianola et al. 2006; Cheng et al. 2010). The special deformation mode for cooperative GB sliding and migration has been built up by Bobylev et al. (2010), which theoretically revealed that the new deformation mode can improve the ductility of nanocrystalline solids in wide ranges of their structural parameters.

However, for nanocrystalline solids containing crack defects, if the stress in the vicinity of a crack tip is large enough, the crack will induce plastic shear through the emission of lattice dislocations from the crack tip. The emission of lattice dislocations along a slip plane can result in blunting of the crack tip, further to hamper crack growth and enhance fracture toughness of nanocrystalline solids. Therefore, it is of great importance to investigate the influence of the cooperative GB sliding and migration on the dislocation emission from a crack tip. In order to do that, Ovid'Ko et al. (2011) theoretically described the operation of cooperative GB sliding and migration process near a tip of growing crack, and analyzed its effect on fracture toughness of nanocrystalline solids. Their results showed that the new deformation mechanism can increase the critical SIF for crack growth and thus enhance the fracture toughness of nanocrystalline solids. Within the model, Feng et al. (2013b) discussed the impact of cooperative GB sliding and migration on dislocation emission from a sharp crack tip by developing a theoretical model in deformed nanocrystalline solids. Thereafter, Feng and her groups (Zhao et al. 2014; Yu et al. 2014) successively presented the effect of cooperative GB sliding and migration on dislocation emission from an elliptically blunt nanocrack tip and a semi-elliptical blunt crack tip.

In general, the researchers mentioned above have been discussing the effect of cooperative GB sliding and migration on dislocation emission from different crack tips, which are usually supposed to be straight or flat. However, real cracks in nanocrystalline solids are relatively complicated and their shapes are various. In fact, an internal crack consisting of a main crack and a branched crack is one usual form of the shapes, and is a more exact description of real cracks compared to straight or flat cracks in nanocrystalline solids. In this paper, we mainly aim to study the effect of cooperative GB sliding and migration on the dislocation emission from the tip of branched crack in deformed nanocrystalline solids.

2 Model and basic problems

The current problem is briefly depicted in Fig. 1a. A deformed nanocrystalline specimen containing an internal crack composed of a main crack and a branched crack with finite length is subjected to mode I loadings and mode II loadings from infinity. The lengths of the main crack and branched crack are denoted by a and b, respectively, and the interior angle between their planes is $(1-m)\pi$. Without loss of generality, we suppose that the length of branched crack is equal to or smaller than that of main crack, namely, $b \leq a$. For simplicity, we make the assumption that the defect structure of the solid remains unchanged along the coordinate axis z perpendicular to the $x - y$ plane, so that the current problem can be dealt with in a two-dimensional plane. At the same time, the key aspects of the problem are capable of being captured in virtue of the described two-dimensional model.

GB sliding and migration near a crack tip can be initiated by the external load and high local stress in the vicinity of a crack tip (Bobylev et al. 2010; Ovid'Ko et al. 2011). The geometry features of the deformation mechanism are schematically shown in Fig. 1b. The cooperative GB sliding and migration can give rise to generation of the sliding distance x and the migration distance y from its initial position BC to a new position DE accompanied by the formation of two disclination dipoles DB_1, CE, which are characterized by the same

strength of opposite signs $\sigma_{yy}-\mathrm{i}\sigma_{xy}=\Phi(\zeta)+\overline{\Phi(\zeta)}+\frac{\omega(\zeta)}{\overline{\omega'(\zeta)}}\overline{\Phi'(\zeta)}+\overline{\Psi(\zeta)}$ and the arm $|x-y|$, y, respectively. In the framework of the theoretical model, we assume that the branched crack tip reaches a triple junction of GBs, and the vertical GB BC is normal to the crack propagation direction and makes an angel δ with the GB AB. The triple junction B lies at a vertical distance p and a horizontal distance q from the branched crack tip A, and the initial length of all grain boundaries is set as d.

For convenience of analysis, the nanocrystalline specimen is supposed to be elastic and isotropic with the shear modulus μ and Poisson's ratio ν. Then, we introduce two Cartesian systems (x_1, y_1), (x_2, y_2) and a polar coordinate (r, θ) with their origins positioned at o_1, o_2, A, respectively. Meanwhile, we let the branched crack lie along x_2 axis. In this case, the coordinates of four disclinations located at the points B, B_1, E and C can be obtained as $z_1(=b+q+r_1e^{\mathrm{i}\theta_1})$, $z_2(=b+q+r_2e^{\mathrm{i}\theta_2})$, $z_3(=b+q+r_3e^{\mathrm{i}\theta_3})$ and $z_4(=b+q+r_4e^{i\theta_4})$, respectively. Here, $r_1(y)=\sqrt{y^2+p^2-2py\cos\delta}$,

$$
\begin{aligned}
r_2(x)&=\sqrt{x^2+p^2-2px\cos\delta},\\
r_3(y)&=\sqrt{y^2+(p+d)^2-2(p+d)y\cos\delta},\\
r_4&=p+d,\\
\theta_1(y)&=-\arccos(y\sin\delta/r_1),\\
\theta_2(x)&=-\arccos(x\sin\delta/r_2),\\
\theta_3(y)&=-\arccos(y\sin\delta/r_3),\quad \theta_4=-\pi/2.
\end{aligned}
$$

For the plane strain problem, stress fields and displacement fields can be described by two Muskhelishvili's complex potentials $\varphi(z)$ and $\psi(z)$ in the complex plane (Muskhelishvili 1977)

$$\sigma_{xx}+\sigma_{yy}=2[\varphi'(z)+\overline{\varphi'(z)}] \tag{1}$$

$$\sigma_{yy}-\mathrm{i}\sigma_{xy}=\varphi'(z)+\overline{\varphi'(z)}+z\overline{\varphi''(z)}+\overline{\psi'(z)} \tag{2}$$

where $z=x+\mathrm{i}y$, the over-bar means a complex conjugate, and the prime denotes derivation with respect to argument z.

For the purpose of solving the current problem more easily, the following mapping function is introduced (Sih 1965)

$$z=\omega(\zeta)=2R(1+\cos\alpha)e^{\mathrm{i}\pi(1-m)}\times\frac{\left(\zeta-\tan\frac{\alpha}{2}\right)^{1+m}\left(\zeta+\tan\frac{\alpha}{2}\right)^{1-m}}{\zeta^2+1} \tag{3}$$

where $\zeta=\xi+\mathrm{i}\eta$. Using Eq. (3), the surrounding region of the internal crack in the z-plane is mapped onto the upper half of the ζ-plane, as shown in Fig. 1c. Furthermore, $\sin\beta=m\sin\alpha$ $(0\le m<1)$, $a=4R\,[\cos(\frac{\alpha+\beta}{2})]^{1-m}[\cos(\frac{\alpha-\beta}{2})]^{1+m}$, $b=4R\,[\sin(\frac{\alpha+\beta}{2})]^{1+m}[\sin(\frac{\alpha-\beta}{2})]^{1-m}$ $(b/a\le 1)$, and R is a real constant. At the same time, α (orβ) can be determined by assigning numerical values to b/a and m.

With the aid of the mapping function in Eq. (3), Eqs. (1) and (2) can be rewritten in the ζ-plane as follows

$$\sigma_{xx}+\sigma_{yy}=2[\Phi(\zeta)+\overline{\Phi(\zeta)}] \tag{4}$$

$$\sigma_{yy}-\mathrm{i}\sigma_{xy}=\Phi(\zeta)+\overline{\Phi(\zeta)}+\frac{\omega(\zeta)}{\overline{\omega'(\zeta)}}\overline{\Phi'(\zeta)}+\overline{\Psi(\zeta)} \tag{5}$$

in which $\Phi(\zeta)=\varphi'(\zeta)/\omega'(\zeta)$, $\Phi'(\zeta)=[\varphi''(\zeta)\omega'(\zeta)-\varphi'(\zeta)\omega''(\zeta)]/[\omega'(\zeta)]^2$ and $\Psi(\zeta)=\psi'(\zeta)/\omega'(\zeta)$.

3 The force on lattice dislocation emission from the tip of branched crack

For the emission of lattice dislocations from the tip of branched crack, we consider a typical situation where the dislocations are of edge character and their Burgers vectors lie along the slip plane making an angle θ with x_1-axis. The force exerted on the edge dislocation is composed of three parts: (1) the force due to the cooperative GB sliding and migration; (2) the image force produced by the internal crack; (3) the applied load.

First, we calculate the force acting on the dislocation produced by the cooperative GB sliding and migration. According to the works of Romanov and Vladimirov (1992) and Zhao et al. (2014), the elastic fields due to two wedge disclination dipoles produced by the cooperative GB sliding and migration in an infinite homogeneous medium can be evaluated by the following complex potentials $\varphi_w(z)$ and $\psi_w(z)$

$$\varphi_w(z)=\frac{D\omega}{2}\sum_{k=1}^{4}s_k(z-z_k)\ln(z-z_k)+\varphi_{w0}(z) \tag{6}$$

$$\psi_w(z)=-\frac{D\omega}{2}\sum_{k=1}^{4}s_k\bar{z}_k\ln(z-z_k)+\psi_{w0}(z) \tag{7}$$

where $D=\mu/[2\pi(1-\nu)]$, $s_1=s_4=1$, $s_2=s_3=-1$, $\varphi_{w0}(z)$ and $\psi_{w0}(z)$ represent the interaction between the two wedge disclination dipoles and the internal crack in the z-plane.

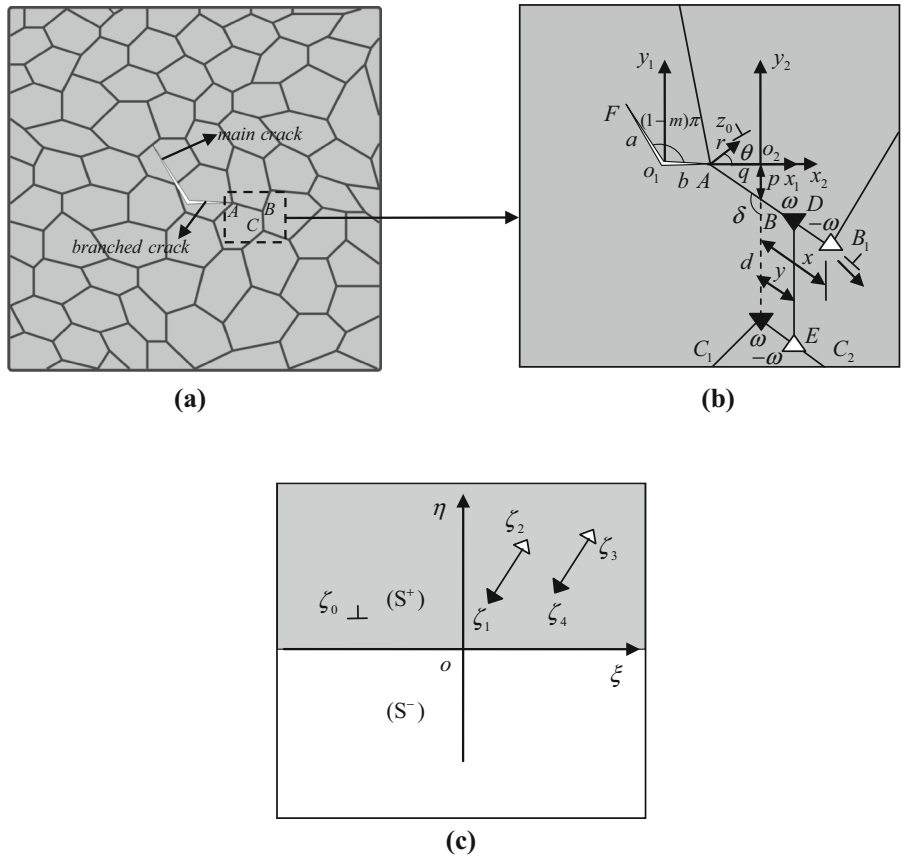

Fig. 1 The cooperative GB sliding and migration in a deformed nanocrystalline specimen with an internal crack consisting of a main crack and a branched crack. **a** General view, **b** two disclination dipoles CE and DB_1 produced by cooperative GB sliding and migration, and a lattice dislocation emitted from the tip of branched crack, **c** the ζ-plane after conformal mapping

With the help of the conformal mapping in Eq. (3), the above Eqs. (6) and (7) can be obtained in the ζ-plane as below

$$\varphi_w(\zeta) = \frac{D\omega}{2}\sum_{k=1}^{4} s_k\omega'(\zeta_k)(\zeta-\zeta_k)\ln(\zeta-\zeta_k) + \varphi_{w0}(\zeta),\ \eta>0 \tag{8}$$

$$\psi_w(\zeta) = -\frac{D\omega}{2}\sum_{k=1}^{4} s_k\bar{z}_k\ln(\zeta-\zeta_k) + \psi_{w0}(\zeta),\ \eta>0 \tag{9}$$

Based on the Riemann-Schwarz symmetry theory, we introduce a new auxiliary function $\chi_w(\zeta)$ as

$$\chi_w(\zeta) = \bar{\omega}(\zeta)\frac{\varphi_w'(\zeta)}{\omega'(\zeta)} + \psi_w(\zeta),\ \eta>0 \tag{10}$$

Substituting Eqs. (8) and (9) into Eq. (10) yields

$$\chi_w(\zeta) = \frac{D\omega}{2}\sum_{k=1}^{4} s_k\left[\bar{\omega}(\zeta)\ln(\zeta-\zeta_k) - \bar{z}_k\ln(\zeta-\zeta_k)\right] + \chi_{w0}(\zeta),\ \eta>0 \tag{11}$$

Referring to Muskhelishvili's treatments, the traction-free boundary condition along the real axis is satisfied by

$$\varphi_w(\zeta) + \frac{\omega(\zeta)}{\overline{\omega'(\zeta)}}\overline{\varphi_w'(\zeta)} + \overline{\psi_w(\zeta)} = 0 \tag{12}$$

To deal with the boundary condition on the interface in Eq. (12), it is convenient for us to introduce the analytic function as follows

$$\Omega_w(\zeta) = -\bar{\chi}_w(\zeta) = \frac{D\omega}{2}\sum_{k=1}^{4} s_k[-\omega(\zeta)\ln(\zeta-\bar{\zeta}_k) + z_k\ln(\zeta-\bar{\zeta}_k)] + \Omega_{w0}(\zeta),\ \eta<0 \tag{13}$$

In combination Eqs. (12) with (13), we can get

$$\varphi_w^+(t) = \Omega_w^-(t) \tag{14}$$

where t denotes the point on the real axis in the ζ-plane. The superscripts "+" and "−" refer to the boundary value as approached from the respective regions occupied by S^+ and S^+.

In view of Eqs. (8) and (13), Eq. (14) can be rewritten as

$$\begin{aligned}&\varphi_{w0}^{+}(t)-\Omega_{w0}^{-}(t)\\&=\frac{D\omega}{2}\sum_{k=1}^{4}s_k\left[-\omega(t)\ln(t-\overline{\zeta_k})+z_k\ln(t-\overline{\zeta_k})\right.\\&\quad\left.-\omega'(\zeta_k)(t-\zeta_k)\ln(t-\zeta_k)\right]\end{aligned}\tag{15}$$

Applying the Plemeij formula, $\varphi_{w0}(\zeta)$ and $\Omega_{w0}(\zeta)$can be calculated by integral along the real axis in the ζ-plane

$$\begin{aligned}\varphi_{w0}(\zeta)&=\frac{D\omega}{2}\sum_{k=1}^{4}s_k\left[-\omega(\zeta)\right.\\&\quad\left.\ln(\zeta-\overline{\zeta_k})+z_k\ln(\zeta-\overline{\zeta_k})\right]\end{aligned}\tag{16}$$

$$\begin{aligned}\Omega_{w0}(\zeta)&=\frac{D\omega}{2}\sum_{k=1}^{4}s_k\omega'(\zeta_k)(\zeta-\zeta_k)\\&\quad\ln(\zeta-\zeta_k)\end{aligned}\tag{17}$$

Inserting Eq. (16) into Eq. (8), we can get

$$\begin{aligned}\varphi_w(\zeta)&=\frac{D\omega}{2}\sum_{k=1}^{4}s_k\left[\omega'(\zeta_k)(\zeta-\zeta_k)\right.\\&\quad\ln(\zeta-\zeta_k)-\omega(\zeta)\\&\quad\left.\ln(\zeta-\overline{\zeta_k})+z_k\ln(\zeta-\overline{\zeta_k})\right]\end{aligned}\tag{18}$$

From Eqs. (13) and (17), the complex potential $\chi_w(\zeta)$is given as

$$\begin{aligned}\chi_w(\zeta)&=\frac{D\omega}{2}\sum_{k=1}^{4}s_k[\overline{\omega}(\zeta)\ln(\zeta-\zeta_k)-\overline{\omega'(\zeta_k)}(\zeta-\overline{\zeta_k})\\&\quad\ln(\zeta-\overline{\zeta_k})-\overline{z_k}\ln(\zeta-\zeta_k)]\end{aligned}\tag{19}$$

Substituting Eqs. (18) and (19) into Eq. (10), we can obtain

$$\begin{aligned}\psi_w(\zeta)&=\frac{D\omega}{2}\sum_{k=1}^{4}s_k\left[-\overline{\omega'(\zeta_k)}(\zeta-\overline{\zeta_k})\right.\\&\quad\left.\ln(\zeta-\overline{\zeta_k})-\overline{z_k}\ln(\zeta-\zeta_k)\right]\\&\quad+\frac{\overline{\omega}(\zeta)}{\omega'(\zeta)}\frac{D\omega}{2}\sum_{k=1}^{4}s_k\left[\omega'(\zeta)\ln(\zeta-\overline{\zeta_k})\right.\\&\quad\left.+\frac{\omega(\zeta)}{\zeta-\overline{\zeta_k}}-\frac{z_k}{\zeta-\overline{\zeta_k}}\right]\end{aligned}\tag{20}$$

The force acting on the edge dislocation produced by two wedge disclination dipoles describing the cooperative GB sliding and migration can be calculated by using the Peach–Koehler formula (Hirth and Lothe 1982)

$$\begin{aligned}f_w&=f_{xw}-\mathrm{i}f_{yw}=\left[\hat{\sigma}_{xy}(\zeta_0)b_x+\hat{\sigma}_{yy}(\zeta_0)b_y\right]\\&\quad+i\left[\hat{\sigma}_{xx}(\zeta_0)b_x+\hat{\sigma}_{xy}(\zeta_0)b_y\right]\\&=\frac{\mu(b_y^2+b_x^2)}{4\pi(1-\nu)}\\&\quad\left[\frac{\Phi_w^{*}(\zeta_0)+\overline{\Phi_{w^*}(\zeta_0)}}{\gamma}+\frac{\overline{\omega(\zeta_0)}\Phi_{w^*\prime}(\zeta_0)+\Psi_{w^*}(\zeta_0)}{\overline{\gamma}}\right]\end{aligned}\tag{21}$$

where $\hat{\sigma}_{xx}$, $\hat{\sigma}_{xy}$ and $\hat{\sigma}_{yy}$ are the components of the stress field due to two wedge disclination dipoles in the process of the cooperative GB sliding and migration deformation, and $\gamma=\mu(b_y-ib_x)/[4\pi(1-\nu)]$.

$$\Phi_w^{*}(\zeta_0)=\lim_{\zeta\to\zeta_0}\left[\frac{\varphi_w'(\zeta)}{\omega'(\zeta)}-\frac{\varphi_{w0}'(\zeta)}{\omega'(\zeta)}\right]$$

$$\begin{aligned}\Phi_{w^*\prime}(\zeta_0)&=\lim_{\zeta\to\zeta_0}\left[\frac{\varphi_w''(\zeta)\omega'(\zeta)-\varphi_w'(\zeta)\omega''(\zeta)}{[\omega'(\zeta)]^3}\right.\\&\quad\left.-\frac{\varphi_{w0}''(\zeta)\omega'(\zeta)-\varphi_{w0}'(\zeta)\omega''(\zeta)}{[\omega'(\zeta)]^3}\right]\end{aligned}$$

$$\Psi_w^{*}(\zeta_0)=\lim_{\zeta\to\zeta_0}\left[\frac{\psi_w'(\zeta)}{\omega'(\zeta)}-\frac{\psi_{w0}'(\zeta)}{\omega'(\zeta)}\right]$$

Second, we assume that the first edge dislocation emitted from the tip of branched crack is located at the point $z_0=b+re^{\mathrm{i}\theta}$ in the $x_1o_1y_1$ coordinate system. According to Fang and Liu (2006) and Fang et al. (2009), the elastic field of edge dislocation in the ζ-plane can be expressed by two complex potentials

$$\varphi_d(\zeta)=\varphi_d^{*}(\zeta)+\varphi_{d0}(\zeta)\tag{22}$$

$$\psi_d(\zeta)=\psi_d^{*}(\zeta)+\psi_{d0}(\zeta)\tag{23}$$

where $\varphi_d^{*}(\zeta)=\gamma\ln(\zeta-\zeta_0)$, $\psi_d^{*}(\zeta)=\overline{\gamma}\ln(\zeta-\zeta_0)-\gamma H/(\zeta-\zeta_0)$ and $H=\overline{\omega(\zeta_0)}/\omega'(\zeta_0)$.

Using the above-mentioned same approach, we have

$$\varphi_d(\zeta)=\gamma\ln(\zeta-\zeta_0)-\gamma\ln(\zeta-\overline{\zeta_0})-\frac{\overline{\gamma}\,\overline{W}}{\zeta-\overline{\zeta_0}}\tag{24}$$

$$\begin{aligned}\psi_d(\zeta)&=\overline{\gamma}\ln(\zeta-\zeta_0)-\frac{\gamma H}{\zeta-\zeta_0}-\overline{\gamma}\ln(\zeta-\overline{\zeta_0})\\&\quad+\frac{\overline{\omega}(\zeta)}{\omega'(\zeta)}\left[\frac{\gamma}{\zeta-\overline{\zeta_0}}-\frac{\overline{\gamma}\,\overline{W}}{(\zeta-\overline{\zeta_0})^2}\right]\end{aligned}\tag{25}$$

where $W=[\overline{\omega}(\zeta_0)-\overline{\omega(\zeta_0)}]/\omega'(\zeta_0)$.

The image force can be calculated by utilizing the Peach–Koehler formula

$$\begin{aligned} f_d &= f_{dx} - \mathrm{i} f_{dy} = \left[\sigma^*_{xy}(\zeta_0)b_x + \sigma^*_{yy}(\zeta_0)b_y\right] \\ &\quad + i\left[\sigma^*_{xx}(\zeta_0)b_x + \sigma^*_{xy}(\zeta_0)b_y\right] \\ &= \frac{\mu(b_y^2 + b_x^2)}{4\pi(1-\nu)}\left[\frac{\Phi^*_d(\zeta_0) + \overline{\Phi^*_d(\zeta_0)}}{\gamma}\right. \\ &\quad \left. + \frac{\overline{\omega(\zeta_0)}\Phi_{d^*\prime}(\zeta_0) + \Psi^*_d(\zeta_0)}{\bar{\gamma}}\right] \end{aligned} \tag{26}$$

where σ^*_{xx}, σ^*_{xy} and σ^*_{yy} are the components of the perturbation stress arising from the interaction between the edge dislocation and the free surface of the internal crack, $\Phi^*_d(\zeta_0) = \varphi_{d^*\prime}(\zeta)/\omega'(\zeta)$, $\Phi_{d^*\prime}(\zeta_0) = \left[\varphi_{d^*\prime\prime}(\zeta_0)\omega'(\zeta_0) - \varphi_{d^*\prime}(\zeta_0)\omega''(\zeta_0)\right]/[\omega'(\zeta_0)]^3$ and $\Psi^*_d(\zeta_0) = \psi_{d^*\prime}(\zeta_0)/\omega'(\zeta_0)$.

Next, the applied load exerted on the edge dislocation can be evaluated by the following equation

$$f_\sigma = b_\perp \sigma_{r\theta} \tag{27}$$

where $b_\perp (= b_x + ib_y)$ is the Burgers vector of the first edge dislocation, $\sigma_{r\theta}$ is in-plane stress induced by remote loadings, and $\sigma_{r\theta} = (\sigma_y - \sigma_x)\sin\theta\cos\theta + \sigma_{xy}(\cos^2\theta - \sin^2\theta)$.

For the linear elastic plane problems, Muskhelishvili (1977) and Neuber (1946) have totally established generalized methods. On the basis of their analyses, Irwin (1957) obtained the well-known equations of the crack-tip stress fields by adopting the first terms of series expansion. Similarly, the solutions to the current problem have been derived as

$$\begin{aligned} \begin{Bmatrix} \sigma_x \\ \sigma_y \\ \sigma_{xy} \end{Bmatrix} &= \frac{K^{app}_{\mathrm{I}}}{\sqrt{2\pi r}}\cos\frac{\theta}{2}\begin{Bmatrix} 1 - \sin\frac{\theta}{2}\sin\frac{3\theta}{2} \\ 1 + \sin\frac{\theta}{2}\sin\frac{3\theta}{2} \\ \sin\frac{\theta}{2}\cos\frac{3\theta}{2} \end{Bmatrix} \\ &\quad + \frac{K^{app}_{\mathrm{II}}}{\sqrt{2\pi r}}\begin{Bmatrix} -\sin\frac{\theta}{2}\left(2 + \cos\frac{\theta}{2}\cos\frac{3\theta}{2}\right) \\ \sin\frac{\theta}{2}\cos\frac{\theta}{2}\cos\frac{3\theta}{2} \\ \cos\frac{\theta}{2}\left(1 - \sin\frac{\theta}{2}\sin\frac{3\theta}{2}\right) \end{Bmatrix} \end{aligned} \tag{28}$$

where K^{app}_{I} and K^{app}_{II} are the applied mode I and mode II SIFs due to infinity load, and (r, θ) is the polar coordinate system whose origin is located at the point A.

Together with Eq. (28), Eq. (27) can be rewritten as below

$$f_\sigma = b_\perp \sigma_{r\theta} = \frac{b_\perp}{\sqrt{2\pi r}}(J_1 K^{app}_{\mathrm{I}} + J_2 K^{app}_{\mathrm{II}}) \tag{29}$$

where $J_1 = \frac{1}{2}\sin\theta\cos\frac{\theta}{2}$, $J_2 = \cos\frac{3\theta}{2} + \sin^2\frac{\theta}{2}\cos\frac{\theta}{2}$.

At last, by using the superposition principle, the total force exerted on the edge dislocation near the tip of branched crack can be calculated as

$$\begin{aligned} f_{emit} &= f_x\cos\theta + f_y\sin\theta + f_\sigma = Re[f_d + f_w] \\ &\quad \cos\theta - Im[f_d + f_w]\sin\theta + f_\sigma \end{aligned} \tag{30}$$

where

$$\begin{aligned} f_d + f_w &= \frac{\mu(b_y^2 + b_x^2)}{4\pi(1-\nu)}\left[\frac{2Re[\Phi^*_d(\zeta_0) + \Phi^*_w(\zeta_0)]}{\gamma}\right. \\ &\quad \left. + \frac{\overline{\omega(\zeta_0)}[\Phi_{d^*\prime}(\zeta_0) + \Phi_{w^*\prime}(\zeta_0)] + [\Psi^*_d(\zeta_0) + \Psi^*_w(\zeta_0)]}{\bar{\gamma}}\right] \end{aligned}$$

4 The critical stress intensity factors for the dislocation emission

It is a broadly accepted criterion that a new dislocation may be spontaneously emitted from a crack tip when the force acting on it is equal to or larger than zero, and the distance between new dislocation and the crack free surface is not smaller than the dislocation core radius r_0 (Rice and Thomson 1974). Associating the Eqs. (18)–(30) and $f_{emit} = 0$, we can obtain the following critical SIFs for dislocation emission

$$\begin{aligned} &K^{app}_{\mathrm{I}} = 0,\ K^{app}_{\mathrm{II}} = \frac{\sqrt{2\pi r}}{b_\perp J_2} \\ &\quad (Im[f_d + f_w]\sin\theta - Re[f_d + f_w]\cos\theta) \end{aligned}$$

for mode II crack, and

$$\begin{aligned} &K^{app}_{\mathrm{II}} = 0,\ K^{app}_{\mathrm{I}} = \frac{\sqrt{2\pi r}}{b_\perp J_1} \\ &\quad (Im[f_d + f_w]\sin\theta - Re[f_d + f_w]\cos\theta) \end{aligned}$$

for mode I crack.

It is worth noting that when the planes of main crack and the branched crack are flattened out into one, namely, for $m = 0$, the present results are qualitatively consistent with the results obtained by Feng et al. (2013b).

The analytical solutions to the current problem have been completely obtained. Next, we examine how cooperative GB sliding and migration affects the dislocation emission from the tip of branched crack by evaluating the critical SIFs in deformed nanocrystalline solids. In the subsequent numerical calculation, we mainly focus on the influences of important parameters such as the lengths of main crack and branched crack, and the angle between their

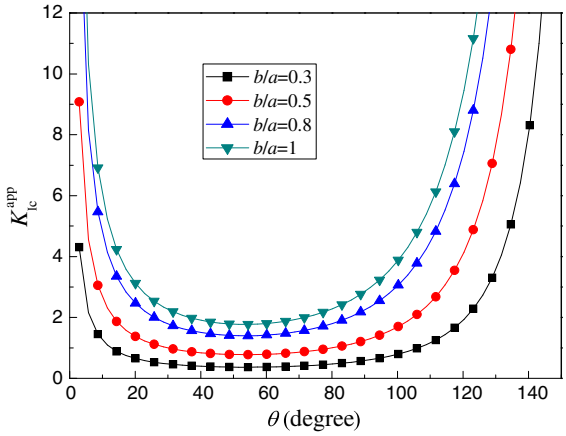

Fig. 2 Normalized critical mode I SIFs versus dislocation emission angle θ with different crack length ratio b/a for $m = 1/3, \omega = \pi/6, x/d = 0.3, y/d = 0.1, \delta = 2\pi/3, p = 0, q = 0, d = 15$nm

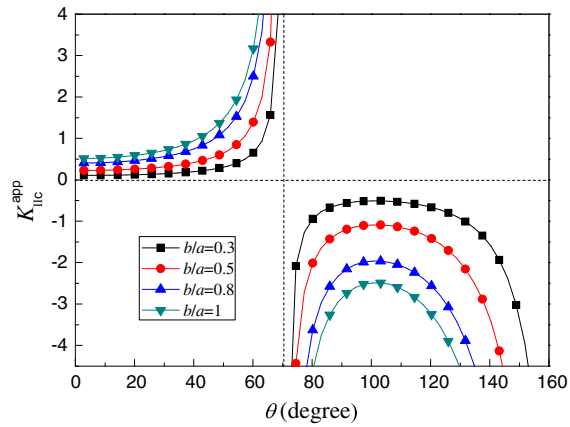

Fig. 3 Normalized critical mode II SIFs versus dislocation emission angle θ with different crack length ratio b/a for $m = 1/3, \omega = \pi/6, x/d = 0.3, y/d = 0.1, \delta = 2\pi/3, p = 0, q = 0, d = 15$nm

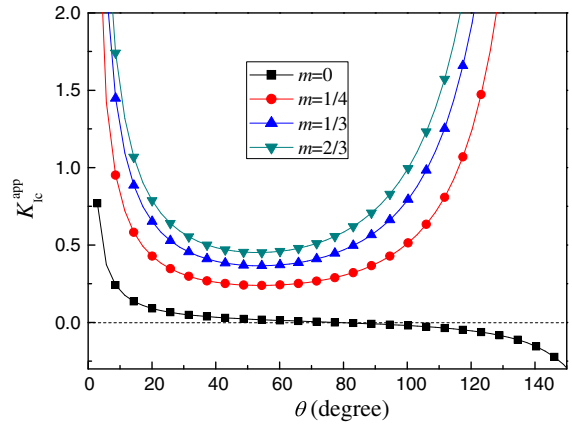

Fig. 4 Normalized critical mode I SIFs versus dislocation emission angle θ with different m for $b/a = 0.3, \omega = \pi/6, x/d = 0.3, y/d = 0.1, \delta = 2\pi/3, p = 0, q = 0, d = 15$nm

planes on the dislocation emission from the tip of branched crack. For simplicity, we define the normalized critical SIFs as $K_{Ic}^{app} = K_{I}^{app}/(\mu R\sqrt{b_{\perp}})$ and $K_{IIc}^{app} = K_{II}^{app}/[\mu R\sqrt{b_{\perp}}]$. Besides, we choose the typical parameter values of the nanocrystalline materials (Hirth and Lothe 1982) Ni with $\mu = 73$Gpa, $\nu = 0.31$ as an illustrative example. As a makeshift, the Burgers vector of the edge dislocation $b = 0.25$nm, and the distance between the tip of branched crack and the emitted dislocation is set as the dislocation core radius r_0 ($r_0 = b/2$).

The variations of the normalized critical SIFs K_{Ic}^{app} and K_{IIc}^{app} versus the dislocation emission angle θ with different crack length ratio b/a are shown in Figs. 2 and 3, respectively. For the normalized critical mode I SIFs in Fig. 2, the normalized critical mode I SIFs first decrease to a minimum from positive infinity, then increase to positive infinity with increasing dislocation emission angle, which suggests that there is a critical angle $\theta_0 = 54.4$ for dislocation emission from the tip of branched crack. It is obvious that the dislocation emission from the tip of branched crack will become more difficult with the increment of the crack length ratio. That is to say, the main crack tends to propagate while shorter branched crack is prone to be blunted by emitting lattice dislocations from its tip, which is qualitatively in line with the results of Feng et al. (2013b). For the normalized critical mode II SIFs depicted in Fig. 3, the normalized critical SIFs increase from a smaller value to infinity, dramatically turn to negative infinity, then increase to a maximum, and finally decrease to negative infinity. According to the work of Huang and Li (2004), the sign of the SIFs depends on the direction of Burgers vector of the emerging dislocations, which means that the normalized critical SIFs can be positive or negative. The most probable angle for positive dislocation emission from the tip of branched crack is always zero, while for negative dislocation emission it is about 100.3°. Furthermore, if the crack length ratio b/a between the branched crack and main crack is larger, the dislocation emission from the tip of branched crack will be more difficult.

The normalized critical mode I and mode II SIFs with respect to dislocation emission angle θ with dif-

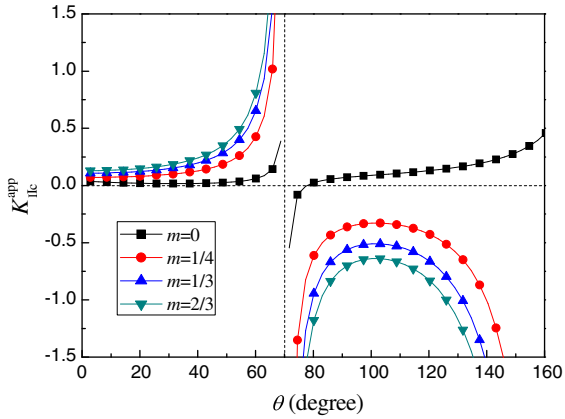

Fig. 5 Normalized critical mode II SIFs versus dislocation emission angle θ with different m for $b/a = 0.3, \omega = \pi/6, x/d = 0.3, y/d = 0.1, \delta = 2\pi/3, p = 0, q = 0, d = 15$nm

ferent m are clearly shown in Figs. 4 and 5, respectively. For the normalized critical mode I SIFs in Fig. 4, it is found that the most probable dislocation emission angle is always 54.4° for $m = 1/4, 1/3$ and 2/3. However, when the planes of main crack and the branched crack are flattened out into one, namely, for $m = 0$, there exists a critical angle 77.3° making the normalized critical SIFs zero, which is in agreement with the results of Feng et al. (2013b). We can also see that when main crack approaches the branched crack, dislocation emission from the tip of branched crack will be suppressed, which means that the two disclination dipoles arising from cooperative GB sliding and migration can shield the dislocation emission from the tip of branched crack. Additionally, we can observe that the dislocation emission from the tip of branched crack is more difficult than from the tip of a single straight crack. For the normalized critical mode II SIFs in Fig. 5, when $m = 1/4, 1/3$ and 2/3, the most probable angle for positive dislocation emission from the tip of branched crack is always zero, while for negative dislocation emission it is nearly 103°. Moreover, when $m = 0$, there is a critical angle 77.3° making the normalized critical SIFs zero, and the dislocation emission from the tip of branched crack is more difficult than from the tip of straight crack.

5 Conclusions

The problem of cooperative GB sliding and migration interacting with an internal crack is investigated by using complex function method. The effect of two wedge disclination dipoles due to cooperative GB sliding and migration on lattice dislocation emission from the tip of branched crack in deformed nanocrystalline materials is theoretically presented. The analytical expressions of the critical SIFs for the first dislocation emission are also derived. Moreover, the influences of vital parameters such as the lengths of branched crack and main crack, and the angle between their planes on the critical SIFs are discussed in detail. In summary, some brief conclusions are listed as follows:

(1) There exists a critical dislocation emission angle near the tip of branched crack, which is independent on the lengths of branched crack and main crack, and mode II loadings are easier to induce dislocation emission from the tip of branched crack than mode I loadings.
(2) When main crack approaches the branched crack, dislocation emission from the tip of branched crack will be suppressed. The main crack tends to propagate while shorter branched crack is prone to be blunted by emitting lattice dislocations from its tip.
(3) Compared with a single straight crack, the dislocation emission from the tip of branched crack is more difficult than from the tip of straight crack.
(4) The grain size, disclination strength and geometry of cooperative GB sliding and migration have great important effect on the critical SIFs.

References

Aifantis EC (2011) Gradient nanomechanics: Applications to deformation, fracture, and diffusion in nanopolycrystals. Metall Mater Trans A 42:2985–2998. doi:10.1007/s11661-011-0725-9

Barai P, Weng GJ (2009) Mechanics of very fine-grained nanocrystalline materials with contributions from grain interior, grain boundary zone, and grain-boundary sliding. Int J Plast 25:2410–2434. doi:10.1016/j.ijplas.2009.04.001

Bhaduri S, Bhaduri SB (1997) Enhanced low temperature toughness of Al_2O_3. Nanostruct Mater 8:755–763. doi:10.1016/S0965-9773(97)00215-8

Bobylev SV, Mukherjee AK, Ovid'Ko IA (2009) Emission of partial dislocations from amorphous intergranular boundaries in deformed nanocrystalline ceramics. Scr Mater 60:36–39. doi:10.1016/j.scriptamat.2008.08.025

Bobylev S, Morozov N, Ovid'ko I (2010) Cooperative grain boundary sliding and migration process in nanocrystalline solids. Phys Rev Lett 105:055504. doi:10.1103/PhysRevLett.105.055504

Bobylev S, Morozov N, Ovid'ko I (2011) Cooperative grain boundary sliding and nanograin nucleation process in nanocrystalline, ultrafine-grained, and polycrystalline

solids. Phys Rev B Condens Matter 84:094103. doi:10.1103/PhysRevB.84.094103
Cheng S, Zhao Y, Wang Y, Li Y, Wang X-L, Liaw PK, Lavernia EJ (2010) Structure modulation driven by cyclic deformation in nanocrystalline NiFe. Phys Rev Lett 104:255501. doi:10.1103/PhysRevLett.104.255501
Dao M, Lu L, Asaro R, De Hosson JTM, Ma E (2007) Toward a quantitative understanding of mechanical behavior of nanocrystalline metals. Acta Mater 55:4041–4065. doi:10.1016/j.actamat.2007.01.038
Fang Q, Liu Y (2006) Size-dependent interaction between an edge dislocation and a nanoscale inhomogeneity with interface effects. Acta Mater 54:4213–4220. doi:10.1016/j.actamat.2006.05.012
Fang Q, Liu Y, Jin B, Wen P (2009) Effect of interface stresses on the image force and stability of an edge dislocation inside a nanoscale cylindrical inclusion. Int J Solids Struct 46:1413–1422. doi:10.1016/j.ijsolstr.2008.11.013
Farrokh B, Khan AS (2009) Grain size, strain rate, and temperature dependence of flow stress in ultra-fine grained and nanocrystalline Cu and Al: Synthesis, experiment, and constitutive modeling. Int J Plast 25:715–732. doi:10.1016/j.ijplas.2008.08.001
Feng H, Fang QH, Zhang LC, Liu YW (2013a) Special rotational deformation and grain size effect on fracture toughness of nanocrystalline materials. Int J Plast 42:50–64. doi:10.1016/j.ijplas.2012.09.015
Feng H, Fang QH, Zhang LC, Liu YW (2013b) Effect of cooperative grain boundary sliding and migration on emission of dislocations from a crack tip in nanocrystalline materials. Mech Mater 61:39–48. doi:10.1016/j.mechmat.2013.02.006
Gianola D, Van Petegem S, Legros M, Brandstetter S, Van Swygenhoven H, Hemker K (2006) Stress-assisted discontinuous grain growth and its effect on the deformation behavior of nanocrystalline aluminum thin films. Acta Mater 54:2253–2263. doi:10.1016/j.actamat.2006.01.023
Gutkin MY, Ovid'Ko IA (2005) grain boundary migration as rotational deformation mode in nanocrystalline materials. Appl Phys Lett 87:251916–251916–251913. doi:10.1063/1.2147721
Hirth JP, Lothe J (1982) Theory of dislocations. Wiley, New York
Huang M, Li Z (2004) Dislocation emission criterion from a blunt crack tip. J Mech Phys Solids 52:1991–2003. doi:10.1016/j.jmps.2004.03.003
Irwin GR (1957) Analysis of stresses and strains near the end of a crack traversing a plate. J Appl Mech 24:361–364
Juan PA, Berbenni S, Capolungo L (2012) Prediction of internal stresses during growth of first- and second-generation twins in Mg and Mg alloys. Acta Mater 60:476–486. doi:10.1016/j.actamat.2011.10.018
Meyers MA, Mishra A, Benson DJ (2006) Mechanical properties of nanocrystalline materials. Prog Mater Sci 51:427–556. doi:10.1016/j.pmatsci.2005.08.003
Morozov N, Ovid'ko I, Sheinerman A, Aifantis E (2010) Special rotational deformation as a toughening mechanism in nanocrystalline solids. J Mech Phys Solids 58:1088–1099. doi:10.1016/j.jmps.2010.04.003
Mukhopadhyay A, Basu B (2007) Consolidation-microstructure-property relationships in bulk nanoceramics and ceramic nanocomposites: a review. Int Mater Rev 52:257–288. doi:10.1179/174328007X160281
Muskhelishvili NI (1977) Some basic problems of the mathematical theory of elasticity. Springer, Berlin. doi:10.1007/978-94-017-3034-1
Neuber H (1946) Theory of notch stresses. JW Edwards, Denver
Ovid'ko IA, Sheinerman AG (2007) Special strain hardening mechanism and nanocrack generation in nanocrystalline materials. Appl Phys Lett 90:171927–171927–171923. doi:10.1063/1.2734393
Ovid'Ko IA, Sheinerman AG (2010) Ductile vs. brittle behavior of pre-cracked nanocrystalline and ultrafine-grained materials. Acta Mater 58:5286–5294. doi:10.1016/j.actamat.2010.05.058
Ovid'Ko IA, Sheinerman AG (2012) Nanoscale rotational deformation near crack tips in nanocrystalline solids. J Phys D Appl Phys 45:335301. doi:10.1088/0022-3727/45/33/335301
Ovid'Ko IA, Sheinerman AG, Aifantis EC (2008) Stress-driven migration of grain boundaries and fracture processes in nanocrystalline ceramics and metals. Acta Mater 56:2718–2727. doi:10.1016/j.actamat.2008.02.004
Ovid'Ko I, Sheinerman A, Aifantis E (2011) Effect of cooperative grain boundary sliding and migration on crack growth in nanocrystalline solids. Acta Mater 59:5023–5031. doi:10.1016/j.actamat.2011.04.056
Rice JR, Thomson R (1974) Ductile versus brittle behaviour of crystals. Philos Mag 29:73–97. doi:10.1080/14786437408213555
Romanov AE, Vladimirov VI (1992) Disclinations in crystalline solids. In: Nabarro FRN (ed) Dislocations in solids, vol 9. North-Holland, Amsterdam, pp 191–402
Sergueeva AV, Mara NA, Krasilnikov NA, Valiev RZ, Mukherjee AK (2006) Cooperative grain boundary sliding in nanocrystalline materials. Philos Mag 86:5797–5804. doi:10.1080/14786430600764906
Sergueeva AV, Mara NA, Mukherjee AK (2007) GB sliding in nanomaterials at elevated temperatures. J Mater Sci 42:1433–1438. doi:10.1007/s10853-006-0697-0
Sergueeva AV, Hulbert DM, Mara NA, Mukherjee AK (2009) Mechanical properties of nanocomposite materials. My Publ 1:127–172. doi:10.1016/B978-0-08-044965-4.50006-7
Sih G (1965) Stress distribution near internal crack tips for longitudinal shear problems. J Appl Mech 32:51–58. doi:10.1115/1.3625783
Wolf D, Yamakov V, Phillpot SR, Mukherjee A, Gleiter H (2005) Deformation of nanocrystalline materials by molecular-dynamics simulation: relationship to experiments? Acta Mater 53:1–40. doi:10.1016/j.actamat.2004.08.045
Wu MS, Zhou K, Nazarov AA (2007) Crack nucleation at disclinated triple junctions. Phys Rev B Condens Matter 76(13):134105
Xia SH, Wang JT (2010) A micromechanical model of toughening behavior in the dual-phase composite. Int J Plast 26:1442–1460. doi:10.1016/j.ijplas.2010.01.005
Xu J, Mao XZ, Xie ZH, Munroe P (2013) Connecting structural, mechanical and tribological characteristics of Al alloyed nanocrystalline molybdenum silicide coatings. J Phys D Appl Phys 46:65304. doi:10.1088/0022-3727/46/6/065304

Yinmin W, Mingwei C, Fenghua Z, En M (2002) High tensile ductility in a nanostructured metal. Nature 419:912–915. doi:10.1038/nature01133

Youssef KM, Scattergood RO, Murty KL, Horton JA (2005) Ultrahigh strength and high ductility of bulk nanocrystalline copper. Appl Phys Lett 87:091904. doi:10.1063/1.2034122

Youssef KM, Scattergood RO, Murty KL, Koch CC (2006) Nanocrystalline Al–Mg alloy with ultrahigh strength and good ductility. Scr Mater 54:251–256. doi:10.1016/j.scriptamat.2005.09.028

Yu M, Fang Q, Feng H, Liu Y (2014) Effect of cooperative grain boundary sliding and migration on dislocation emitting from a semi-elliptical blunt crack tip in nanocrystalline solids. Acta Mech 225:1–15. doi:10.1007/s00707-013-1039-3

Zhao Y, Qian J, Daemen LL, Pantea C, Zhang J, Voronin GA, Zerda TW (2004) Enhancement of fracture toughness in nanostructured diamond-SiC composites. Appl Phys Lett 84:1356–1358. doi:10.1063/1.1650556

Zhao Y, Fang Q, Liu Y (2014) Effect of cooperative nanograin boundary sliding and migration on dislocation emission from a blunt nanocrack tip in nanocrystalline materials. Philos Mag 94:700–730. doi:10.1080/14786435.2013.861091

Zhou K, Wu MS, Nazarov AA (2008) Relaxation of a disclinated tricrystalline nanowire. Acta Mater 56:5828–5836. doi:10.1016/j.actamat.2008.07.059

Zhu L, Zheng X (2010) Influence of interface energy and grain boundary on the elastic modulus of nanocrystalline materials. Acta Mech 213:223–234. doi:10.1007/s00707-009-0263-3

Zhu YT, Liao XZ, Wu XL (2012) Deformation twinning in nanocrystalline materials. J Mater Eng Perform 57:1–62. doi:10.1016/j.pmatsci.2011.05.001